ARCHIVES of
Computational Materials Science and Surface Engineering

International Scientific Journal
published quarterly by the Association of Computational Materials Science and Surface Engineering

2009 • Volume 1 • Issue 2 • 112-119

A comparative study on the damage initiation mechanism of elastomeric composites

T. Da Silva Botelho*, N. Isac, E. Bayraktar
School of Mechanical and Manufacturing Engineering,
Supmeca/LISMMA-Paris, EA 2336, St-Ouen, France
* Corresponding author: E-mail address: tony.dasylva@supmeca.fr

Received in a revised form 11.10.2007; published 15.02.2009

ABSTRACT

Purpose: Modelling – Finite Element Analysis (FEA) of the damage initiation mechanisms in thin rubber sheet composites were carried out under static solicitation at room temperature. Natural rubber vulcanised and reinforced by carbon, NR is used in this study.

Design/methodology/approach: Experimental results were compared with that of the Finite Element Analysis (FEA). Damage mechanism has been described with a threshold criterion to identify the tearing resistance, characteristic energy for tearing (T) and damage in the specimens was evaluated just at the beginning of the tearing by assuming large strain. A typical type of specimen geometry of thin sheet rubber composite materials was considered under static tensile tests conducted on the smooth and notched specimens with variable depths. In this way, the effects of the plane stress on the damage mechanism are characterized depending on the rubber materials.

Findings: In this stage of this research, a finite element analysis (FEA) has been applied under the same conditions of this part in order to obtain the agreement between experimental and FEA results. The numerical modelling is a representation of a previous experimental study. The specimen is stretched more than once its initial size, so that large strains occur. A hyper elastic Mooney-Rivlin law and a Griffith criterion are chosen. The finite elements analysis was performed with ABAQUS code (V.6.4.4). The tearing energy is evaluated with contour integrals. The Griffith criterion states that a notch with an initial length will elongate of a differential length for a given strain state only if the variation of elastic energy is higher than the variation of the surface energy related to the newly created surface.

Practical implications: A tearing criterion was suggested in the case of simple tension conditions by assuming large strain. In the next step of this study, a finite element analysis (FEA) will be applied under the same conditions of this part in order to obtain the agreement between experimental and FEA results.

Originality/value: This study proposes a threshold criterion for the damage just at the beginning of the tearing for thin sheet rubber composites and gives a detail discussion for explaining the damage mechanisms. Comparison of FEA results with those of experimental studies gives many facilities for the sake of simplicity in industrial application.

Keywords: Rubber composites; Finite Element Analysis; Damage mechanism; Static solicitation; Plane stress; Tearing energy

Reference to this paper should be given in the following way:

T. Da Silva Botelho, N. Isac, E. Bayraktar, A comparative study on the damage initiation mechanism of elastomeric composites, Archives of Computational Materials Science and Surface Engineering 1/2 (2009) 112-119.

METHODS OF ANALYSIS AND MODELLING

1. Introduction

Considering a natural rubber (NR) in static tensile loading, the applied stress is increased sufficiently high and evidently a tearing will begin to develop from a stress-raising defect, frequently in one edge, and eventually it reaches the other side, breaking the specimen in two pieces [1-5]. Griffith's theory of fracture of an elastic solid indicates that a crack, once started, will grow forward rapidly, because the strain energy released by growth increases continuously as the crack grows. But, in practice, the crack often takes a surprising deviation path, especially in the initial stages. It turns sharply into a direction parallel to the applied stress (sideways), instead of going forward, and grows for some distance in this unexpected direction before coming to a halt. When the applied stress is increased further, a new crack tip appears, pointing in the forward direction, but again it quickly turns sideways, parallel to the applied stress, grows for some distance in this direction, and then stops. This process may be repeated several times before a crack forms that grows across the specimen and breaks it in two pieces [6-24].

Design and chose of an elastomeric material for a specific usage requires determining precisely the mechanical behaviour of this material. This determination includes four-step processes. First one has to find the models that are able to fit with the ranking of materials. This step is based on a bibliographic study and a good knowledge of the mechanics of elastomeric materials. The second step requires an experimental study of the materials according to a specific usage[9,13,15,24].

This stage is well adapted to select the most suitable behaviour model among those selected in the first stage. It also allows determining the numerical values of the mechanical parameters of the selected model. The third step consists in a numerical modelling of the experimental study, so as to validate the choice of the mechanical model and the determination of its constants. In the last step, it is satisfactory to model numerically the final usage of the material, so as to produce an accurate dimensioning.

This paper is related on the third stage of the formerly exposed process in the study of damage initiation mechanism of Natural Rubber (NR) composite strips [12,14-16].

The numerical modelling consists in a quasi-static uniaxial tension on a thin rectangular notched rubber specimen. This modelling aims at validate the mechanical behaviour model of NR and evaluate the associated strain energy, so as to determine the limit load for a given thickness.

In fact, the numerical modelling is a representation of a preceding experimental study. The specimen is stretched very heavily from its initial size, so that large strains occur. A hyper elastic Mooney-Rivlin law is chosen. The finite elements analysis (FEA) was performed with ABAQUS code (V.6.4.4). The strain energy is evaluated integrating the force-displacement curve (post-treatment of the finite elements analysis).

The numerical modelling is a representation of a previous experimental study. The specimen is stretched (deformed) very heavily from its initial size, so that very large strains occur. That is why; a hyperelastic Mooney- Rivlin law and a Griffith criterion are chosen. The finite elements analysis was performed with ABAQUS code (V.6.4.4).

The tearing energy is evaluated with contour integrals. The Griffith criterion states that a notch with an initial length will elongate of a differential length for a given strain state only if the variation of elastic energy is higher than the variation of the surface energy related to the newly created surface:

$$-\frac{dW}{dc} > T.\frac{dA}{dc} \tag{1}$$

where dW is the variation of elastic energy, T is the surface energy per unit of surface of the material, dc is the differential elongation of the notch and dA is the area resulting of the elongation.

2. Damage initiation mechanism in NR

Damage in the specimens for NR evaluated by SEM just at the beginning of the tearing, have been studied and published in detail in the first part of this study [15,16]. Detail discussion on the NR specimens will be given in the present paper. As explained in the [15,16], static tensile samples were drawn only up to the beginning of the crack propagation and then stopped the machine. The samples were kept constant at this position by means of a special device having a quick locking system where special cover has been arranged and then, the entire setting is placed in SEM for the examinations.

The SEM photomicrographs show the damage initiation mechanism and/or the evolution of too early beginning of the crack propagation for the NR in a state of plane stresses as a convex form at the bottom of crack of the samples (Figures 1a, b, c and d). Crystallisation phenomenon is typically observed all of the composition of the NR samples (Figure 1c). Because crystallisation phenomenon give an additional effect to decreases the tearing energy of NR samples.

Additionally, the presence of small openings/holes is well detected as shown in the Figure 1d. These are in reality the micro cavitations just before the crack propagation that play an important role in final damage of the rubber composites.

The development of the cavities occur too early beginning of the deformation at the bottom of the edge notch of the specimen and final rupture take shape only from one of the well developed cavities. These evolutions have been observed on the different compositions of NR composites that explain the damage initiation mechanism under static solicitation.

Additives that considerably support bonding of carbon black to rubber have been shown to reduce both hysteretic losses and fracture strength. On the other hand, it is expected that an extremely weak interaction is undesirable, since, even though slippage could readily occur, little energy would be spent in the process.

Based on the above opinions, there would seem to be an optimum level of adhesion between rubber and filler for the best reinforcement, although the desired interaction may depend on the particular fracture conditions that influence the damage initiation under solicitation of the materials.

The results obtained on the NR (it crystallises when loaded) samples under static solicitation, give a clear idea that the structure and additive elements play a major role on the fracture behaviour – failure modes of these materials. This is a basic idea to explain the damage initiation in NR composites sheets.

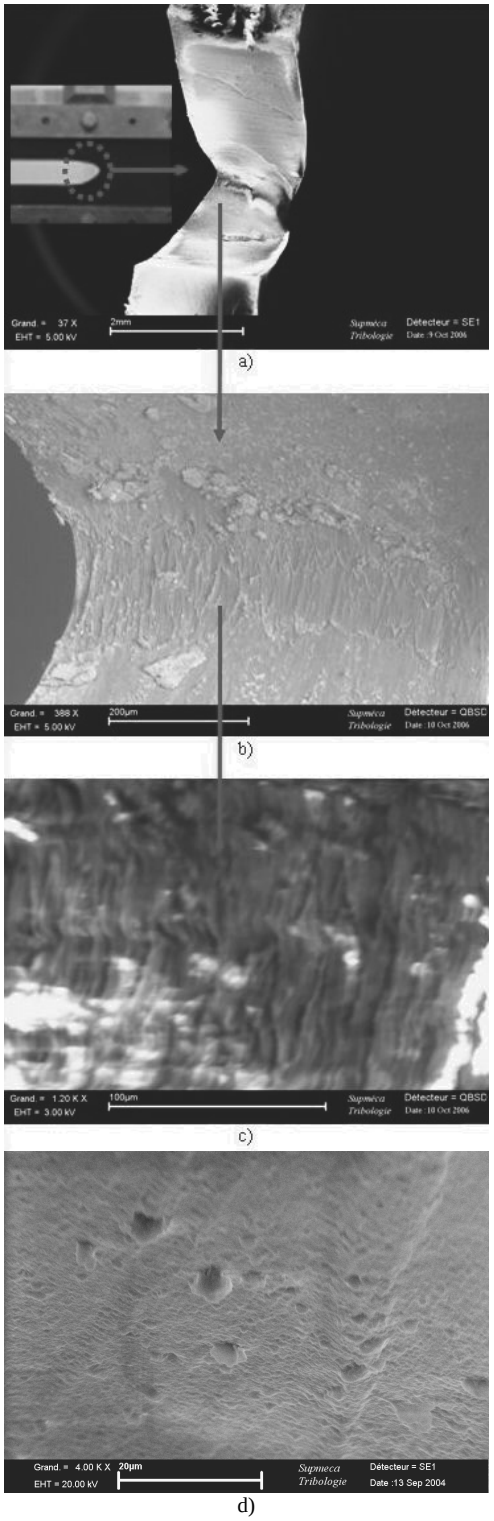

Fig. 1. SEM photomicrographs showing the beginning of the crack propagation at the bottom of NR specimen (a, b and c); formation of the micro cavities at the bottom of the notch too early at the beginning of the crack propagation of NR (d)

Thus, some interesting interactions between the structure, chains and additive elements occurred in the rubber composites can explain the evolution of the tearing and or critical tearing energy in the NR structures.

In the present paper, damage mechanism will be discussed by means of FEA and the results obtained by modelling will be compared with those of the experimental.

3. Finite elements model

The geometry of the smooth (without notch) specimen has been indicated in Figure 2.

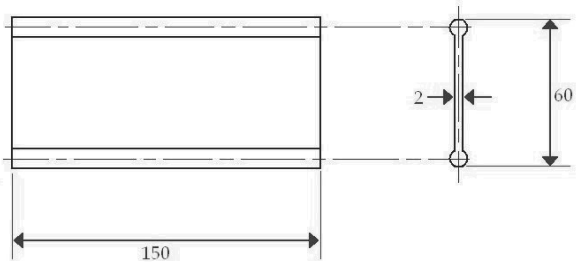

Fig. 2. Geometry of the smooth specimen

The notch is then made at one end, through the symmetry plane of the specimen with an initial length, c, and is submitted to a uniaxial tension. Notched specimen loading path and crack deviation phenomenon under uniaxial tension have been presented in Figures 3a and 3b.

a)

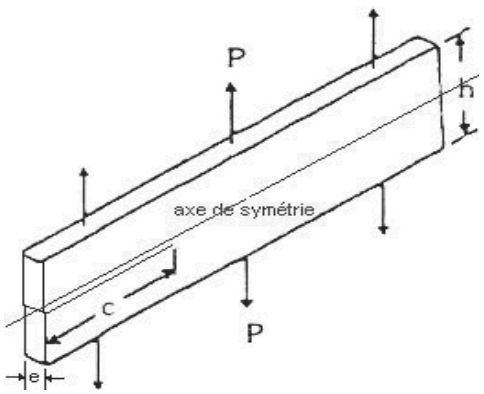

b)

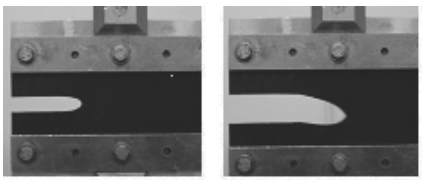

Fig. 3. Notched specimen loading path a) and crack deviation phenomenon under uniaxial tension b)

According to the symmetry of the model, only half of the geometry can be modeled. In addition, due to the thinness of the specimen, a plane stress situation should be taken into account.

In order to perform the contour integrals and compute the tearing energy, the geometrical model is partitioned into nine concentric circles that they are centered at the notch front.

Geometrical sets are then associated with each contour. During the post-treating, one will be able to extract and compute easily the quantities necessary to evaluate the tearing energy. These partitions also allow applying a more regular meshing of the model around the notch front (Figure 4).

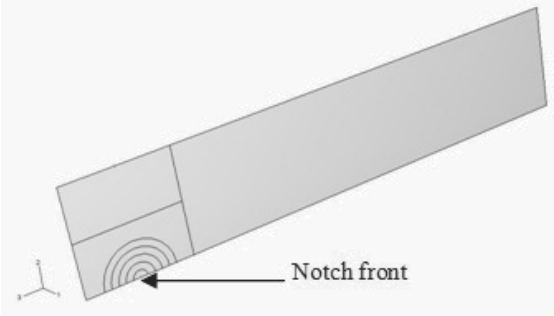

Fig. 4. Partition of the geometry of half of the specimen with a notch size of 15mm

3.1. Material

The Natural rubber experiences a second order hyper elastic Mooney-Rivlin law, whose coefficients have been identified from the former experimental studies [12,14-16]. The coefficients of the law have been summarized in Table 1.

Table 1.
Coefficients of the Mooney-Rivlin law

Coefficient	Value
C10	0.295788
C01	-0.018755
C20	0.014761
C11	0.
C02	0.
D1	0.000967
D2	0.

3.2. Boundary conditions and loading

Since only half of the geometry is modelled, one has to introduce the symmetry boundary conditions. These have to be applied to the lower face of the specimen excepting the specimen has been notched, so that the notch lips remain free.

On the upper side of the specimen, a 30 mm vertical displacement is imposed.

3.3. Mesh analysis

A mesh seed was imposed on the geometrical boundaries and on the partition lines. The circular partitions made around the notch front were seeded with 23 nodes regularly spaced.

A rectangular partition was also made to connect this circular-shaped meshing with the mesh of the other parts of the specimen, which was regularly meshed. The meshing was then performed using linear quadrangular elements (Figure 5).

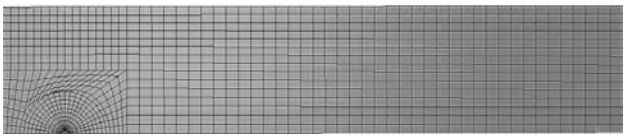

Fig. 5. Meshing of the specimen

The model has 1119 nodes, corresponding to 1052 elements and a total 6714 DOF.

4. Finite elements results and analysis

Calculations were made on a PC (Pentium 4, 3 GHz, 1 GB RAM) and required 13.3 s CPU time and 8.30 GB disk space. After calculation the results are examined using ABAQUS post-treatment tools and then data concerning the nine contours are extracted to be post-treated using Matlab.

Figure 6 gives the displacement in the tension direction and the maximum principal stresses are observed around the notch front as indicated in Figure 7.

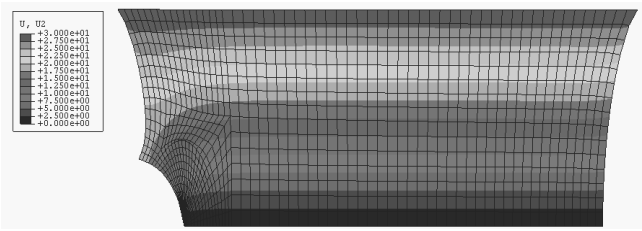

Fig. 6. Displacement in the tension direction (scale factor: 1.0)

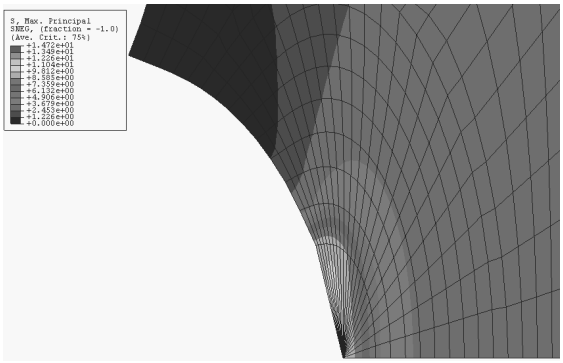

Fig. 7. Maximum principal stress (detail around the notch front)

4.1. Energy calculations

The strain energy is classically defined as the area under the force-displacement curve. For each length of the notch, a 30 mm ramp displacement was applied along the 1 s step time. This means that the step time parameter (ranging from 0 to 1) allows determining for each increment the applied displacement.

Therefore, with one single load case, and using the results for each increment, the whole force-displacement curve was deduced (discredited using the step-time parameter) [9,11,15,18,19,21].

Thus, the post-treating of the FEA gave for each displacement level the associated total reaction force. An integration of the force-displacement curve (Figure 8) was performed, giving a strain energy–displacement curve (Figure 9).

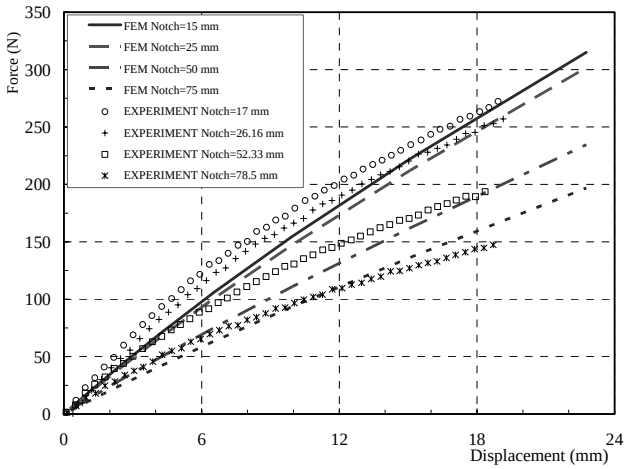

Fig. 8. Comparison of tension test results of the smooth and notched specimens of NR specimens with different edge cracks

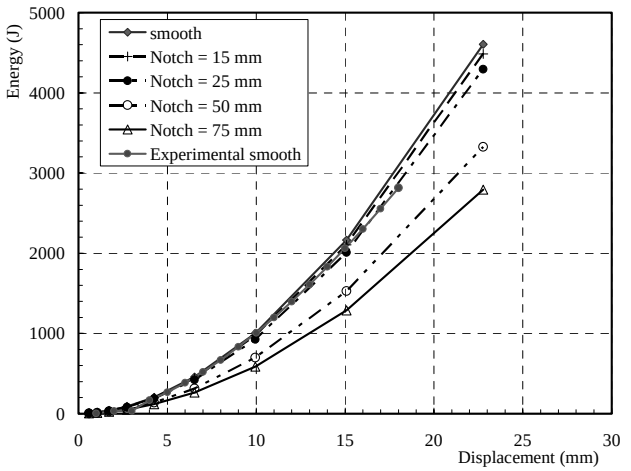

Fig. 9. Evolution of the tearing energy depending on the displacement for NR specimen

From the analysis of Figure 9, it is shown that the smaller values of the notch size give the higher strain energy levels, which is also an experimental result. In addition, the displacement-energy curves exhibit a second order polynomial shape.

These numerical results were then compared to the experimental data. Figure 10 indicates a comparison of the strain energy between numerical and experimental results for the notch lengths ranging from 0 to 50 mm and for the given tension displacements ranging from 5 to 18 mm. The whole numerical results were shown to be in accord with experimental observations of elastic stored energy depending on the length of the edge crack for the given displacements.

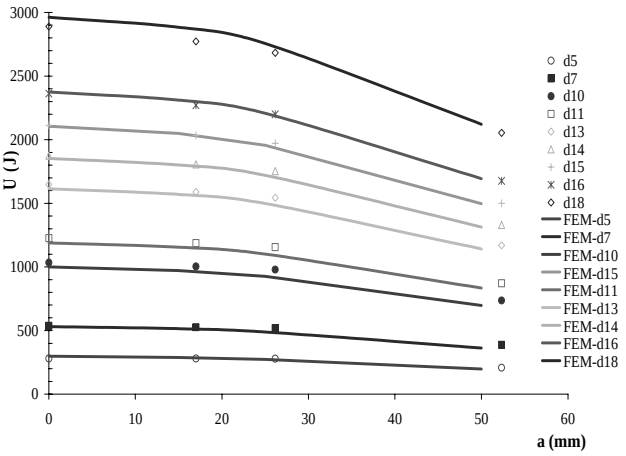

Fig. 10. Elastic stored energy depending on the length of the edge crack for a given displacement for NR specimens

Additionally, the J-integrals have been evaluated on each arc circle. Generally, they are given in the following form:

$$J = \int_{\Gamma+} W(M) - \vec{T}(M).\frac{\partial \vec{u}}{\partial x}(M) ds \tag{2}$$

These are decomposed into two terms:

$$\begin{aligned} J &= J_1 - J_2 \\ J_1 &= \int_{\Gamma+} W(M)\, ds \\ J_2 &= \int_{\Gamma+} \vec{T}(M).\frac{\partial \vec{u}}{\partial x}(M)\, ds \end{aligned} \tag{3}$$

J_1 is the strain energy and J_2 is related to the tension vector, $T_i = \sigma_{ij} n_j$. For commodity, the integrals are performed using cylindrical coordinates. In this coordinate system, the strain components are defined as the following form and they have been illustrated in Figure 11:

$$\begin{cases} \varepsilon_{xx} = \dfrac{\partial u}{\partial x} = \dfrac{\partial u}{\partial r}\cos\theta - \dfrac{1}{r}\dfrac{\partial u}{\partial \theta}\sin\theta \\ \varepsilon_{yy} = \dfrac{\partial v}{\partial y} = \dfrac{\partial v}{\partial r}\sin\theta + \dfrac{1}{r}\dfrac{\partial v}{\partial \theta}\cos\theta \\ \varepsilon_{xy} = \dfrac{1}{2}\left(\dfrac{\partial u}{\partial y} + \dfrac{\partial v}{\partial x}\right) = \dfrac{1}{2}\left[\left(\dfrac{\partial u}{\partial r} - \dfrac{1}{r}\dfrac{\partial v}{\partial \theta}\right)\sin\theta + \left(\dfrac{\partial v}{\partial r} + \dfrac{1}{r}\dfrac{\partial u}{\partial \theta}\right)\cos\theta\right] \end{cases} \tag{4}$$

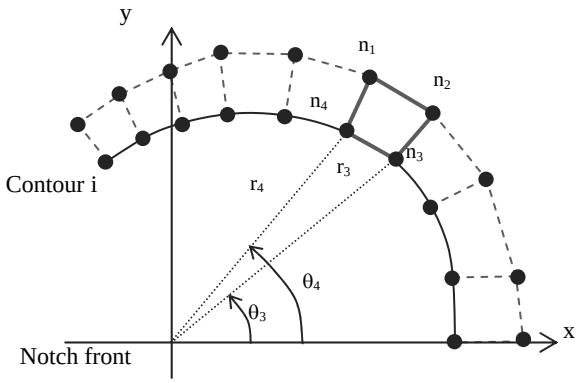

Fig. 11. Cylindrical coordinate system for the contours

These two energy terms are computed each with data extracted from the finite elements analysis. Since these results are discrete, an interpolation has to be performed to evaluate the J-integral. According to the refinement of the meshing, a θ-linear interpolation is assumed along the path of each contour.

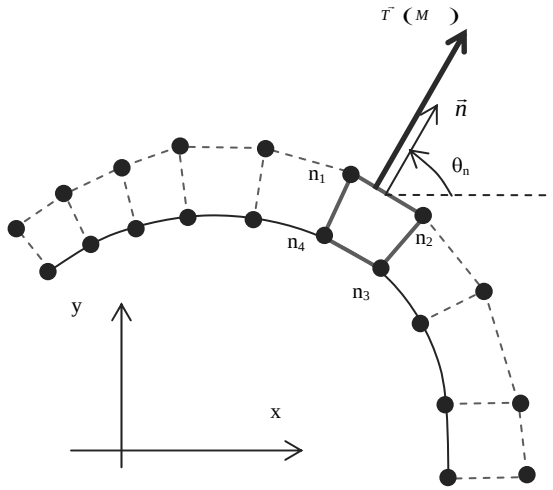

Fig. 12. Orientation of the tension vector

The derivatives are also evaluated using finite differences. An example taken from Figure 11 and also Figure 12 give:

$$\frac{\partial u_3}{\partial r}=\frac{u_2-u_3}{r_2-r_3} \quad ; \quad \frac{\partial u_3}{\partial \theta}=\frac{u_4-u_3}{\theta_4-\theta_3}$$
$$\frac{\partial v_3}{\partial r}=\frac{v_1-v_3}{r_1-r_3} \quad ; \quad \frac{\partial v_3}{\partial \theta}=\frac{v_4-v_3}{\theta_4-\theta_3} \tag{5}$$

The term J_1 is then evaluated according to plane stress assumptions (Eq. 6):

$$J_1=\int_{\Gamma+} W(M)ds=\int_{\Gamma+}\frac{1}{2}\left(\sigma_{xx}\varepsilon_{xx}+\sigma_{yy}\varepsilon_{yy}\right)+\sigma_{xy}\varepsilon_{xy}ds \tag{6}$$

Since stresses and strains are θ-linearly interpolated (i.e. $\sigma_{ij}=\lambda_{\sigma_{ij}}\theta+C_{\sigma_{ij}}$ and $\varepsilon_{ij}=\lambda_{\varepsilon_{ij}}\theta+C_{\varepsilon_{ij}}$), Eq. 6 leads to perform the integration of a constant coefficients θ second-order polynomial function. The final expression of J_1 is a third-order θ polynomial function which form is given in Eq. 7.

$$J_1=\int_{\Gamma+} W(\theta)d\theta=\alpha_3\theta^3+\alpha_2\theta^2+\alpha_1\theta \tag{7}$$

To evaluate J_2, one needs an expression for the tension vector, $\vec{T}(M)$, and the derivative term $\frac{\partial \vec{u}}{\partial x}(M)$ (Figure 12).

For a given element, such as presented in Figure 12, the definition of the tension vector is:

$$\vec{T}\left(\vec{n}\right)=\sigma_{ij}n_j=\begin{Bmatrix}\sigma_{xx}\cos\theta_n+\sigma_{xy}\sin\theta_n\\ \sigma_{xy}\cos\theta_n+\sigma_{yy}\sin\theta_n\end{Bmatrix} \tag{8}$$

With defining $\cos\theta_n$ and $\sin\theta_n$;

$$\cos\theta_n=\frac{y_1-y_2}{L_{n_1n_2}} \quad ; \quad \sin\theta_n=\frac{x_1-x_2}{L_{n_1n_2}} \tag{9}$$

Additionally, from Equation 4, $\frac{\partial \vec{u}}{\partial x}$ can be identified as the following form;

$$\frac{\partial \vec{u}}{\partial x}=\begin{Bmatrix}\frac{\partial u}{\partial x}\\ \frac{\partial v}{\partial x}\end{Bmatrix}\begin{Bmatrix}\frac{\partial u}{\partial r}\cos\theta-\frac{1}{r}\frac{\partial u}{\partial \theta}\sin\theta\\ \frac{\partial v}{\partial r}\cos\theta-\frac{1}{r}\frac{\partial v}{\partial \theta}\sin\theta\end{Bmatrix} \tag{10}$$

In addition to the stresses θ-linearly interpolated, it is assumed that $\frac{\partial u}{\partial x}$ and $\frac{\partial v}{\partial x}$ are linear functions of θ too. Thus the term $\vec{T}.\frac{\partial \vec{u}}{\partial x}$ is written as a second order θ polynomial function:

$$\vec{T}.\frac{\partial \vec{u}}{\partial x}=d_2\theta^2+d_1\theta+d_0 \tag{11}$$

where d_i are constant coefficients.

As a consequence, the J_2 integral is a third order polynomial function with constant coefficients.

After the evaluation of the J_1 and J_2, the J-integral can then be calculated for each of the eight contours: $J=J_1-J_2$.

Figure 13 shows the evolution of the J-integral computation from the data extracted from the finite elements analysis through the contours. As indicated in this figure, the main contribution to J is provided by the J_1 term.

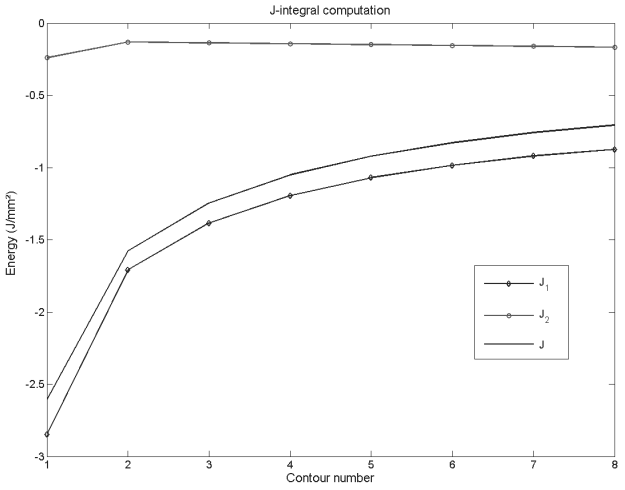

Fig. 13. J-integral computation from the data extracted from the finite elements analysis

The model proposed here and the results are news and a little work was found in the literature. This model gives a simple threshold criterion for the damage just at the beginning of the tearing for thin sheet rubber composites and gives. Comparison of FEA results with those of experimental studies gives many facilities for the sake of simplicity in industrial application.

5. Conclusions

A comparative study was carried out on the modelling – Finite Element Analysis (FEA) of the damage initiation mechanisms in thin rubber sheet composites under static solicitation at room temperature. Natural rubber vulcanised and reinforced by carbon, NR is used in this study.

The FEA results have been compared with those of experimental. Some major trends can be underlined from this comparative study:

- This work gives a threshold criterion for the damage just at the early beginning of the damage for thin sheet rubber composites. The stresses are the basic reasons at the edge crack well before the crack propagation both in forcing the materials to relocate and in orientation effects, in other words, crack deviation mechanism always occur in the rubber composites.
- Crystallisation phenomenon give an additional effect to decreases the tearing energy of NR samples. Cavitation formed at early beginning of the deformation has also a major effect on the damage mechanisms for NR materials.
- For the design purposes of the NR composite applications, the second order Moonley-Rivlin law coefficients was chosen to describe the mechanical behaviour. In the present work, this law was implemented for FEA.
- The strain energy was particularly analyzed, since it is a relevant parameter for failure criteria. The comparison of experimental and numerical results has been shown to be in accord with damage initiation in rubber thin strip composites with chosen mechanical law for the damage initiation.

Acknowledgements

The authors thank Mr. M.A. Helleboid, Mr. O. Thao and Mr. R. Luong for contribution obtained during their graduating research work at LISMMA in Supmeca- Paris.

References

[1] A.N. Gent, M.R. Kashani, Why do cracks turn sideways, Rubber Chemistry and Technology 76 (2001) 122-131.
[2] H.W. Greensmith, The change in Stored Energy on Making a Small Cut in a Test Piece held in Simple Extension, Journal Polymer Science 7 (1963) 993-1002.
[3] G.J. Lake, Fatigue and fracture of elastomers, Rubber Chemical Technology 66 (1995) 435-460.
[4] P.B. Lindley, Energy for crack growth in model rubber components, Journal Strain Analysis 7 (1972) 132-140.
[5] R.S. Rivlin, A.G. Thomas, Rupture of Rubber. Part 1: Characteristic energy for tearing, Journal of Polymers Sciences 10 (1953) 291-318.
[6] E. Bayraktar, F. Montembault, C. Bathias, Damage Mechanism of Elastomeric Matrix Composites, Proceedings of the Conference "Experimental Mechanics", 2005, Portland, Oregon, USA.
[7] E. Bayraktar, K. Bessri, C. Bathias, Deformation behaviour of elastomeric matrix composites under static loading conditions, Journal of Engineering Fracture Mechanics 75/1 (2007) (On line).
[8] T. Da Silva Botelho, N. Isac, E. Bayraktar, Modelling of damage initiation mechanism in rubber sheet composites under the static loading, Journal of Achievements in Materials and Manufacturing Engineering 22/2 (2007) 55-58.
[9] J.R. Cho, J.I. Song, K.T. Noh, D.H. Jeon, Nonlinear finite element analysis of swaging process for automobile power steering hose, Journal of Materials Processing Technology 170/1-2 (2005) 50-57.
[10] H. Ghaemi, K. Behdinan, A. Spence, On the development of compressible pseudo-strain energy density function for elastomers: Part 1. Theory and experiment, Journal of Materials Processing Technology 178/1-3 (2006) 307-316.
[11] H. Ghaemi, K. Behdinan, A. Spence, On the development of compressible pseudo-strain energy density function for elastomers: Part 2. Application to FEM, Journal of Materials Processing Technology 178/1-3 (2006) 317-327.
[12] M.A. Helleboid, O. Thao, Modeling of tearing of the rubber specimens under static solicitations, BSc, SUPMECA-Paris/LISMMA, Paris, 2006.
[13] S. Jerrams, K. Sanders, K.B. Goo, Realistic modelling of earthquake-isolation bearings, Journal of Materials Processing Technology 118/1-3 (2001) 158-164.
[14] R. Luong, Study of the tearing of thin rubber sheets and double cantilever beam (DCB) rubber specimens under static solicitations, MSc, SUPMECA-Paris/LISMMA, Paris, 2005.
[15] R. Luong, N. Isac, E. Bayraktar, Damage initiation mechanism in rubber sheet composites during the static loading, Archives of Materials Science and Engineering 28/1 (2007) 19-26.

[16] R.Luong, N. Isac, E. Bayraktar, Failure mechanisms in thin rubber sheet composites under static solicitation, Journal of Achievements in Materials and Manufacturing Engineering 21/1 (2007) 43-46.
[17] M.H. Makled, T. Matsui, H. Tsuda, H. Mabuchi, M.K. El-Mansy, K. Morii, Magnetic and dynamic mechanical properties of barium ferrite–natural rubber composites, Journal of Materials Processing Technology 160/2 (2005) 229-233.
[18] R.M.V. Pidaparti, Finite element analysis of interface cracks in rubber materials, Engineering Fracture Mechanics 47 (1994) 309-316.
[19] R.M.V. Pidaparti, T.Y. Yang, W. Soedel, A plane stress FEA for the prediction of rubber fracture, International Journal of Fracture 39 (1989) 255-268.
[20] P.V.M. Rao S.G. Dhande, A flexible surface tooling for sheet-forming processes: conceptual studies and numerical simulation, Journal of Materials Processing Technology 124/1-2 (2002) 133-143.
[21] G. Wróbel, S. Pawlak, Ultrasonic evaluation of the fibre content in glass/epoxy composites, Journal of Achievements in Materials and Manufacturing Engineering 18 (2006) 187-190.
[22] J.H. Wu, J.L. Huang, N.S. Chen, C. Wei, Y. Chen, Preparation of modified ultra-fine mineral powder and interaction between mineral filler and silicone rubber, Journal of Materials Processing Technology 137/1-3 (2003) 40-44.
[23] J. Yan, J.S. Strenkowski, A finite element analysis of orthogonal rubber cutting, Journal of Materials Processing Technology 174/1-3 (2006) 102-108.
[24] R. Zulkifli, L.K. Fatt, C.H. Azhari, J. Sahari, Interlaminar fracture properties of fibre reinforced natural rubber/polypropylene composites, Journal of Materials Processing Technology 128/1-3 (2002) 33-37.